

## RESEARCH ARTICLE

# Predicting photopolymer resin pyrolysis kinetics in ceramic vat photopolymerization additive manufacturing

Eoin G. McAleer | Joseph Prati | John M. Matthewson | Richard A. Haber |  
Enver Koray Akdoğan 

Department of Materials Science and Engineering, Rutgers University, Piscataway, New Jersey, USA

## Correspondence

Enver Koray Akdoğan, Department of Materials Science and Engineering, Rutgers University, Piscataway, NJ 08854, USA.

Email: [eka@soe.rutgers.edu](mailto:eka@soe.rutgers.edu)

## Funding information

National Science Foundation, Grant/Award Number: 1540027

## Abstract

The kinetics of polymers pyrolysis, particularly those containing ethoxylated trimethylolpropane triacrylate ((EtO)<sub>3</sub>-TMTPA), is of utmost importance in optimizing the binder removal process that is associated with ceramic vat photopolymerization (CerVPP). Here, we focus on the decomposition kinetics of a simplified resin, which is a photopolymer system that is formulated from (EtO)<sub>3</sub>-TMTPA and a photoinitiator (diphenyl(2,4,6-trimethylbenzoyl) phosphine oxide). The thermal behavior of the resin was critically assessed with the use of thermogravimetric analysis (TGA) under atmospheric pressure in a flowing argon gas atmosphere. The Fraser–Suzuki function was used to deconvolve the TGA peaks in conjunction with nonlinear regression that was based on a finite difference solution of the nonlinear rate equation. From this analysis, pertinent kinetic parameters were obtained. The variation of the kinetic parameters was studied as a function of heating rate. The resulting model allowed for the prediction of thermal decomposition behavior of CerVPP resins for a representative, simulated, yet practical heating rate program. This prediction was compared to TGA measured resin decomposition using the same heating rate program. The model's predictions accurately identified the two primary apparent reaction steps displayed in the differential TGA data.

## KEYWORDS

additive manufacturing, kinetics, photopolymerization, polymers, pyrolysis

## 1 | INTRODUCTION

Ceramic vat photopolymerization (CerVPP) is a leading technique for creating intricate ceramic parts.<sup>1</sup> While CerVPP holds advantages over traditional ceramic processing methods, it is a polymer-based method that involves a lengthy binder removal process, that is, debinding.<sup>1</sup> The

debinding step in ceramic manufacturing is often carried out based on trial and error. It is a time-consuming and potentially problematic process<sup>2</sup> because the binder, in this case a photopolymer resin, must be removed from the CerVPP part slowly enough to prevent specimen failure.<sup>1–3</sup>

Debinding parts fabricated with CerVPP is particularly challenging compared to other ceramic processing

This is an open access article under the terms of the [Creative Commons Attribution-NonCommercial](https://creativecommons.org/licenses/by-nc/4.0/) License, which permits use, distribution and reproduction in any medium, provided the original work is properly cited and is not used for commercial purposes.

© 2025 The Author(s). *Journal of the American Ceramic Society* published by Wiley Periodicals LLC on behalf of American Ceramic Society.

methods. The forming process requires the use of a high volumetric loading of polymer, often exceeding 50% by volume.<sup>3</sup> This means that a large volume of generated gas must be expelled from the green body during debinding. Methods such as tape casting and ceramic injection molding face a similar set of problems.<sup>4</sup> An additional challenge with CerVPP debinding is the high thermal stability of cured photopolymers.<sup>5,6</sup> This stability implies a wider range of polymer degradation and a higher final debinding temperature. These cured polymers are thermosets and do not redistribute in the body during firing leading to a nonuniform removal of the binder system.<sup>7</sup>

In principle, a thorough understanding of the fundamental aspects of the thermal decomposition in CerVPP parts can streamline the debinding process. The study of resin decomposition is typically accomplished with the use of thermogravimetric analysis (TGA).<sup>3–5</sup> As the resin undergoes thermal treatment, rapid formation of gaseous reaction products can occur via thermal decomposition, leading to defects in the ceramic green bodies.<sup>8</sup> Predicting green body fracture would necessitate an understanding of the internal pressure development in the green body during debinding. The removal of resin from the particle network is often diffusion limited so the system must be designed accordingly.<sup>9</sup> Incorporating the role of pressure in green body failure modeling has been accomplished by other authors and would be a logical next step to include in future studies.<sup>10</sup>

Thermal debinding can be conducted in a variety of gas atmospheres depending on the chemistry of both the resin and the ceramic.<sup>11</sup> Oxidizing atmospheres such as air are often used because air furnaces are cheap, and both degradation of the resin and removal of carbon are achieved in a single processing step. Inert gas in the form of argon or nitrogen is often used to avoid some of the oxidation reactions that can lead to increased gas output.<sup>12</sup> Thermal decomposition in inert and non-oxidizing atmospheres is referred to as pyrolysis. Pyrolysis of acrylic resins has been studied previously and has been found to involve a combination chain end scission at low temperature and random chain scission at high temperature.<sup>13</sup> Although incorporating the relevant chemical mechanisms into the model would strengthen its reliability, this is excluded at this time to make this model more relevant to a ceramic engineer that may not fully understand the numerous chemical interactions during thermal debinding in the, often proprietary, resins that are used in CerVPP.<sup>14</sup>

The thermal decomposition of polymers is typically analyzed through the prism of chemical kinetics, where the approach is to assess the rates at which chemical reactions occur as a function of temperature and time. In this study, we endeavor to develop an understanding of the thermal decomposition kinetics of a simplified CerVPP

resin. Applying kinetic analysis to TGA data, the developed model will aim to predict the thermal decomposition of CerVPP resins. Predicting resin decomposition at a variety of heating rates with only a few experiments can allow the ceramic engineer to more rapidly develop thermal debinding protocols for CerVPP parts.

The field of reaction kinetics is vast with many different methodologies being applied successfully.<sup>15</sup> Each approach has its advantages, usually a tradeoff between ease of use, accuracy, and complexity. Many studies approximate reactions as containing a single reaction step,<sup>16–20</sup> which greatly simplifies the approach at the cost of accuracy.<sup>21</sup> In many cases, this approximation is sufficient as there is rate limiting step in many thermal decomposition reactions.<sup>22</sup> On the other hand, the single step model may be insufficient when dealing with large mixtures of components, each with multiple degradation steps, as is often the case in CerVPP. Hence, here, the focus is on the use of a multistep kinetic model to describe the thermal decomposition of a CerVPP resin. The proposed approach combines peak deconvolution and nonlinear regression with a non-analytical rate equation. Gaining insight into thermal decomposition of CerVPP resins can pave the way for more precise and expedited debinding cycles, leading to defect-free ceramic parts that can be sintered to high density.

## 2 | KINETICS FORMALISM

To develop the model, we first introduce the relevant kinetics concepts and parameters of interest for chemical processes involving a constant heating rate such as thermal decomposition of polymers. The ensuing presentation applies to a single reaction rate equation only. The rates of thermal decomposition reactions are parameterized as a function of temperature ( $T$ ), degree of conversion ( $\alpha$ ), and pressure ( $P$ ).<sup>15</sup> While pressure is a component of the comprehensive rate equation, it is disregarded in this study due to the challenges associated with measuring the partial pressure of individual reactants.<sup>15</sup> The rate equation used in this study has the following mathematical form:

$$\frac{d\alpha}{dt} = k(T) f(\alpha) \quad (1)$$

Here, the reaction rate constant  $k(T)$  has an Arrhenius type of dependence on temperature given by

$$k(T) = Ae^{\frac{-E_a}{RT}} \quad (2)$$

where  $A$  is the pre-exponential factor or frequency factor,  $E_a$  is the apparent activation energy,  $R$  is the ideal gas

constant, and  $T$  is the absolute temperature. The function  $f(\alpha)$  represents the conversion rate of the reaction products and is modeled according to a chosen reaction model.<sup>4,8,10</sup> In this study, we chose a power law reaction model:

$$f(\alpha) = (1 - \alpha)^n \quad (3)$$

where  $n$  is the reaction order. The experiments used in this study to determine the kinetic parameters were conducted at a constant heating rate  $\beta$ , which we define as follows:

$$\beta = \frac{dT}{dt} \quad (4)$$

Equations (1)–(4) can be combined to give the rate law used in this study

$$\frac{d\alpha}{dT} = \beta A \exp\left(\frac{-E_a}{RT}\right) (1 - \alpha)^n \quad (5)$$

Equation (5) is a differential equation that cannot be solved analytically. Therefore, it is necessary to either find an approximate analytical solution or to solve it using numerical methods. There are two main approaches to study the kinetics of decomposition reactions: (1) model-free methods and (2) model fitting methods.<sup>15</sup> These two categories can also be further subdivided into integral and differential methods depending on which form of the differential equation is used and on the type of data the computations are being made.

Model-free methods have many different forms and are extensively used in this field.<sup>13,18,19,23–33</sup> Such methods rely on the isoconversional principle, which states that the reaction rate at a constant extent of conversion is only a function of temperature.<sup>24</sup> These methods require the use of multiple heating rate experiments and the determination of the activation energy at multiple values of conversion.<sup>15</sup> The Friedman method is the widely used method for the differential isoconversional techniques.<sup>28</sup> This method does not use approximations. However, the process of transforming TGA data into differential data by numerical differentiation will unavoidably introduce noise. In addition, inaccuracies will be introduced in the process if data smoothing is used, which is typical.<sup>15</sup> On the other hand, integral methods in model-free kinetics formalisms may not require manipulation of TGA data.<sup>23</sup> However, they often require the use of approximations to the integral form of the differential equations. The common methods in this category are the Flynn–Wall–Ozawa (FWO) method, Kissinger–Akahira–Sunose (KAS) method, and the method developed by Vyazovkin.<sup>18,19,23,33</sup> Both FWO and KSA use approximations in the general form  $\ln\left(\frac{\beta_i}{T_i^n}\right) =$

$C_0 - C_1\left(\frac{E_a}{RT}\right)$ .<sup>15</sup> Vyazovkin was able to use numerical integration to further improve on the integral methods.<sup>15,33</sup> Model-free methods are valuable for their ease of application but are known to be valid over small ranges of conversion.<sup>15</sup>

Model fitting methods take a different approach to solving for the kinetic parameters by defining a function  $f(\alpha)$  to describe a given decomposition reaction. Such methods either use linear or nonlinear regression to determine the kinetic parameters.<sup>5–7</sup> The most popular linear model fitting methods for thermal decomposition are those of Coats and Redfern<sup>16</sup> and Lee and Beck.<sup>17</sup> Both methods rely on simplifying the integral form of the differential equation by approximations. While Coats and Redfern approximate an asymptotic series, Lee and Beck carries out integration by parts assuming some terms are negligible.<sup>5,6</sup> Both methods then assume a kinetic model to determine the corresponding kinetic parameters. However, such methods require a choice of reaction order that is arbitrary or needs repeated fits to the data to determine the optimal reaction order.<sup>5,6</sup> While the linear methods have proven useful in specific scenarios, the complexity and diversity of many reactions necessitate more adaptable and comprehensive techniques.

In this study, we utilized nonlinear model fitting methods which, in contrast to isoconversional and linear model fitting methods, can handle multistep reactions and intricate kinetics. Our approach adopts an  $n$ th order reaction model to articulate the rate dependence on conversion,<sup>34</sup> building on the work of Prati et al.<sup>35</sup> The technique employed here is based on nonlinear regression using a finite difference method to the associated differential equation. Notably, our method employs a trust region reflective algorithm (TRRA) for the optimization of least squares in lieu of the standard Levenberg–Marquardt algorithm used by conventional methods.<sup>36,37</sup>

Accordingly, we solved Equation (5) using TRRA. Because the TGA measures the mass remaining ( $m$ ) and not the degree of conversion ( $\alpha$ ), where  $m = (1 - \alpha)$ , the finite difference approach was used to solve the equation as per:

$$m_i = m_{i-1} + \left(\frac{dm}{dT}\right)_{i-1} (T_i - T_{i-1}) \quad (6)$$

By substituting Equation (5) into Equation (6), one obtains

$$m_i = m_{i-1} - \left(\frac{Am_{i-1}^n}{\beta}\right) \exp\left[\frac{-E_a}{RT_{(i-1)}}\right] (T_i - T_{i-1}) \quad (7)$$

Equation (7) enables computation of the estimated mass,  $m_i$ , for every temperature  $T_i$  by utilizing the preceding

estimated mass,  $m_{i-1}$ , the kinetic parameters of each reaction,  $A$ ,  $E_a$ ,  $n$ , and the heating profile  $\{T_i\}$ . The formula is then aligned with the observed masses,  $\{M_i\}$ , using a nonlinear least-squares regression technique (TRAA) that is executed in MATLAB via the `lsqcurvefit` function. This approach determines the kinetic parameters of the reaction  $A$ ,  $E_a$ , and  $n$ .

Moreover, to tackle more complex reaction kinetics, we incorporated peak deconvolution of the differential thermogravimetric (DTG) data into our methodology. When utilized for a single reaction system, our technique offers a representation of the ongoing chemical reactions. However, one must acknowledge that chemical processes, especially thermal decomposition reactions, are seldom restricted to a single reactive step.<sup>38</sup> Ideally, every step in a reaction is distinctly identifiable in experimental data. On the other hand, singling out each reaction often proves to be a challenge in practice if not impossible. Even within DTG data, where reactions manifest themselves as distinct steps, it is common to find multiple reactions contributing to a singular apparent peak on a DTG plot. As such, it becomes imperative to dissect the overall reaction data into clusters that represent singular reactions. For the purposes of this study, we consider data manifesting as singular degradation peaks in the DTG signal to be individual reactions. While this might seem to be an oversimplification, such an approach enables the description of a vast spectrum of decomposition reactions without delving into the intricacies of each underlying reaction. This approach holds value for practitioners aiming to streamline the thermal decomposition process across various binder systems in CerVPP.

Deconvolution is used to address apparent reaction step overlap in the DTG data. The existing kinetics literature points to two prominent forms of kinetic deconvolution: (1) mathematical deconvolution analysis (MDA) and (2) kinetic deconvolution analysis (KDA).<sup>21</sup> The MDA method was used in this study to deconvolve reaction peaks where the underlying assumption is that each apparent reaction step is independent from each other. While there might be exceptions to this assumption in each ensemble of thermal decomposition reactions, our choice of deconvolution of DTG peaks aligns with our aim of crafting a generalized methodology to streamline analyses for CerVPP systems.

To apply MDA to DTG data a peak shape function (PSF) must be chosen to accomplish the deconvolution of reaction peaks. The choice of PSF is of paramount importance for obtaining accurate fits to the kinetic data. We implemented the Fraser–Suzuki function in our analyses because it has been proven to be very successful in fitting various reaction kinetics data.<sup>26,39–41</sup> The Fraser–Suzuki

function is given by

$$F(t) = a_0 \exp \left[ -\ln 2 \left\{ \frac{\ln \left( 1 + 2a_3 \left( \frac{t-a_1}{a_2} \right) \right)}{a_3} \right\} \right] \quad (8)$$

$a_0$ ,  $a_1$ ,  $a_2$ , and  $a_3$  are the parameters corresponding to the amplitude, position, half-width, and asymmetry of the peak, respectively.<sup>42,43</sup> The Fraser–Suzuki function was used within MATLAB to deconvolve the DTG data. This deconvolution follows the steps first reported by O’Haver.<sup>44</sup>

Deconvolution requires the estimation of parameters describing the PSF. The initial values for the parameters of each apparent reaction step were determined using mouse inputs on a graph of the DTG data. Approximate locations of the DTG peak maximum and the two values at the half maximum of each curve were chosen. The approximate DTG peak maximum was used as a guess for  $a_1$ , the difference in the approximate half maximum values was used as a guess for  $a_2$ , and a value of zero is used as a guess for  $a_3$ . The  $a_0$  parameter is not needed as an input parameter because the function implemented in MATLAB will solve for the amplitude of each peak. Once these initial guesses were determined, the “`fminsearch`” function in MATLAB was used to find the parameters that minimize the error between the DTG data and the description of the DTG peak using the Fraser–Suzuki function. The “`fminsearch`” function utilizes the simplex search method established by Lagarias using the Nelder–Mean algorithm.<sup>45</sup>

Once the Fraser–Suzuki function describing each peak in the DTG data is established, the function describing each DTG peak is evaluated at each point of the temperature data vector from the TGA experiment. The nonlinear curve fitting, described above, is then performed on the data for each apparent reaction step to provide values for  $A$ ,  $E_a$ , and  $n$ . These kinetic parameter values can then be used to give an overall description of the reaction rate by substituting them into the finite difference description of the reaction rate. Again, assuming that the reactions are independent, the descriptions of the reaction rate for each independent apparent reaction can be summed in the following way for  $m$  reactions:

$$\frac{d\alpha}{dt} = \sum_i^m k_{i(T)} f_{i(\alpha)} \quad (9)$$

It will be shown that the nonlinear model fitting can be used to comprehensively analyze multistep reactions. This study distinguishes itself by employing a combination of the Fraser–Suzuki function and non-linear model fitting to analyze thermal decomposition phenomena in CerVPP

systems via TGA, offering an alternative to conventional isoconversional methods.

### 3 | EXPERIMENTAL METHODS

#### 3.1 | Sample preparation and curing

A photopolymer resin was prepared for this study, which will be referred to as M100. This resin consists of a combination of a photoreactive monomer (ethoxylated trimethylolpropane triacrylate [(EtO)<sub>3</sub>-TMTPA]) and a photoinitiator (diphenyl(2,4,6-trimethylbenzoyl) phosphine oxide [TPO]). The mixture consists of 97% by weight of (EtO)<sub>3</sub>-TMTPA and 3% by weight of TPO. To mix the resin, the constituents were added to a 250 mL container and mixed in a dual asymmetric centrifugal mixer (Flacktek Inc.). Three aluminum oxide grinding media were added to aid the mixing process. The mixing cycle was conducted in four stages which were all conducted under 2 kPa of pressure. The four stages had the following mixing rates 17.5, 20.8, 32.5, and 20 Hz and were for 2, 2, 1, and 1 min, respectively. Mixing was repeated until TPO was fully incorporated, and resin was no longer cloudy. This resin contains elements common to resins used in the additive manufacturing of aluminum oxide. No ceramic powder was included in the resin to eliminate effects from solid loading or surface interactions between the ceramic and polymer.

The resins underwent a curing process, which was accomplished using the DLP light engine (3DLP9000 light engine; Digital Light Innovations) contained within the Admaflex 130 (Admatec Inc.) 3D printer. A sheet of biaxially oriented polyethylene terephthalate was placed on top of the glass that resided above the projector. A vat was placed above the polymer film, and a thick layer of resin was poured into the vat. A 405 nm light was projected onto the resin with an energy dose of 150 J/m<sup>2</sup>. A mask consisting of a 4 × 8 array of 4.5 mm circles was used to obtain cured resin samples that fit easily into the pans used for thermal analysis.

#### 3.2 | Thermogravimetric analysis and differential scanning calorimetry

TGA was conducted using a TA Instruments SDT 650 following the guidelines provided by the ICTAC Kinetics Committee.<sup>46</sup> The range for TGA analysis was between 295 and 1073 K. A range of heating rates were used, that is, 0.5, 1, 10, and 50 K/min. The atmosphere control was accomplished with argon gas (Airgas Ultra High Purity Grade) at 100 mL/min flow rate. Argon is used to prevent sig-

nificant oxidation during debinding.<sup>13</sup> The TGA chamber was left at room temperature under flowing gas for 30 min before the experiment was started. Alumina crucibles were used in the TGA analyses of resin samples. Sample mass remained around 40 mg.

The derivative of the data was computed numerically using the gradient function in MATLAB. The spacing of the points to which the gradient operation was applied was varied depending on heating rate. Such an approach was needed to correct for the fact that the sampling rate at each heating rate was left constant. The spacing in points for heating rates of 0.5, 1, 10, and 50 K/min were 466, 233, 23, and 4, respectively.

### 4 | RESULTS AND DISCUSSION

The analysis reported below utilized data collected via TGA under flowing argon at heating rates of 0.5, 1, 10, and 50 K/min. Figure 1 shows the TGA experiments and the derived DTG data. Upon inspecting the data, several observations stand out:

1. As the heating rate rises, the degradation onset shifts to a higher temperature as commonly observed in TGA analysis.<sup>37</sup>
2. The maximum mass loss rate per unit temperature (K) remains relatively constant.
3. The number of noticeable DTG peaks differs depending on the heating rate. At a 0.5 K/min heating rate, three distinct apparent reaction steps are visible, reaching maximum rates at around 633, 669, and 803 K. At a 50 K/min heating rate, the first two peaks in the DTG signal merge into a single apparent reaction step. This apparent reaction step reaches a maximum rate of mass loss at approximately 743 K. The DTG signal at high temperatures also shows a notable reduction in its maximum degradation rate at this heating rate.

As elaborated in Section 2, the multistep kinetic analysis requires peak deconvolution using the Fraser–Suzuki function to characterize each local DTG signal peak. Since the 0.5 K/min heating rate offered the most discernible apparent reaction steps in its degradation behavior, these data served as a visual indicator for determining the reaction steps required for modeling. Given the three local DTG signal maxima at the 0.5 K/min rate, three apparent reaction steps were used as the basis of the degradation kinetics model.

Beginning with the slowest heating rate of 0.5 K/min, the data are first deconvolved into three functions, each representing one apparent reaction step. The subsequent three heating rate experiments are analyzed, using the

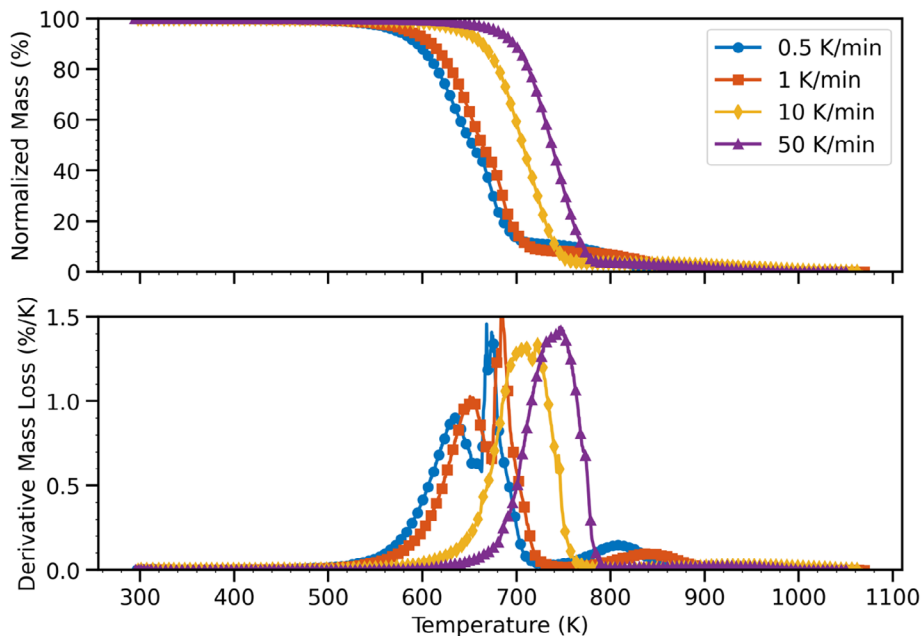


FIGURE 1 Thermogravimetric analysis (TGA) and differential thermogravimetric (DTG) data as a function of heating rates for M100 ceramic vat photopolymerization (CerVPP) 3D printing resin.

parameters derived from the initial rate experiment as starting estimates for characterizing the three apparent reaction steps. The objective was to maintain the relative positioning of the apparent reaction steps consistent across different heating rates. It is worth noting that the two fastest heating rate experiments result in the merging of the two previously distinct peaks in the DTG data observed at slower rates. The resulting deconvolved peaks and the raw DTG data are shown in Figure 2.

After describing the deconvolved peaks in the DTG data using the Fraser–Suzuki function, the next step was to fit the empirical Fraser–Suzuki curves with the kinetic description of each apparent reaction. This is achieved by using nonlinear regression to a finite difference solution of the kinetic differential equations to obtain the kinetic parameters that fit the Fraser–Suzuki description of each apparent reaction step. Data generated for fitting purposes are created by solving the Fraser–Suzuki representation of each apparent reaction step with the experimental data's temperature dependence. The reaction order was confined to the 0–2 interval.

In Figure 3, each peak is depicted by its Fraser–Suzuki function representation (solid line) and its corresponding kinetic description (dotted line), with the apparent reaction steps grouped by their respective heating rates. One immediately notices that the established kinetic parameters describe the Fraser–Suzuki function representations of the apparent reaction steps well, although there is some discrepancy at the second peak for slower heating rates of 0.5 and 1 K/min. This discrepancy could be

TABLE 1 Kinetic parameters as a function of heating rate for M100 resin.

	Peak weight	$\ln(A)$	$E/R$	$n$
0.5°C/min heating rate				
Peak 1	0.59	14.02	14 123.5	0.898
Peak 2	0.31	80.23	58 984.46	1.99
Peak 3	0.1	26.29	27 718.66	1.4
1°C/min heating rate				
Peak 1	0.6	18.18	16 634.41	0.89
Peak 2	0.32	90.26	66 345.01	1.99
Peak 3	0.08	23.13	25 665.86	1.4
10°C/min heating rate				
Peak 1	0.67	28.62	23 480.28	0.898
Peak 2	0.3	96.26	73 226.43	1.99
Peak 3	0.03	12.6	17 399.57	1.4
50°C/min heating rate				
Peak 1	0.65	32.18	25 908.73	0.898
Peak 2	0.31	98.07	76 236.38	1.99
Peak 3	0.04	10.23	13 052.53	1.4

attributed to the fact that descriptions with a reaction order below 2 have difficulties in accurately capturing the sharp degradation rate observed in peak 2.

Table 1 contains the kinetic parameters characterizing each apparent reaction step. When substituted into the finite difference description from Equation (7), it enables the calculation of the predicted conversion as a function of temperature. This prediction is set against the raw TGA

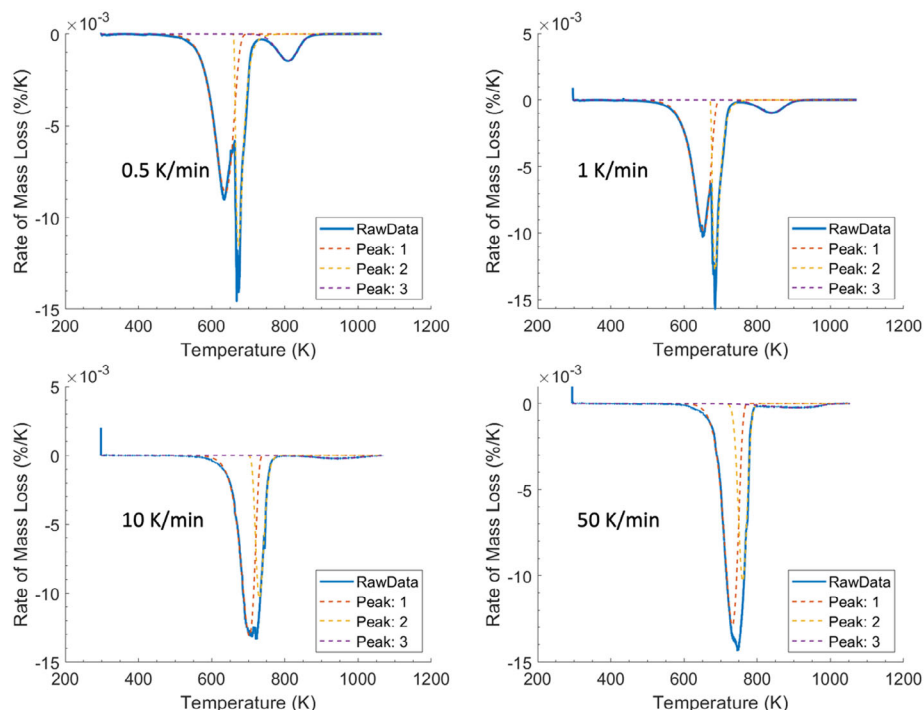


FIGURE 2 Deconvolution of differential thermogravimetric (DTG) profiles as a function of heating rate for M100 ceramic vat photopolymerization (CerVPP) 3D printing resin.

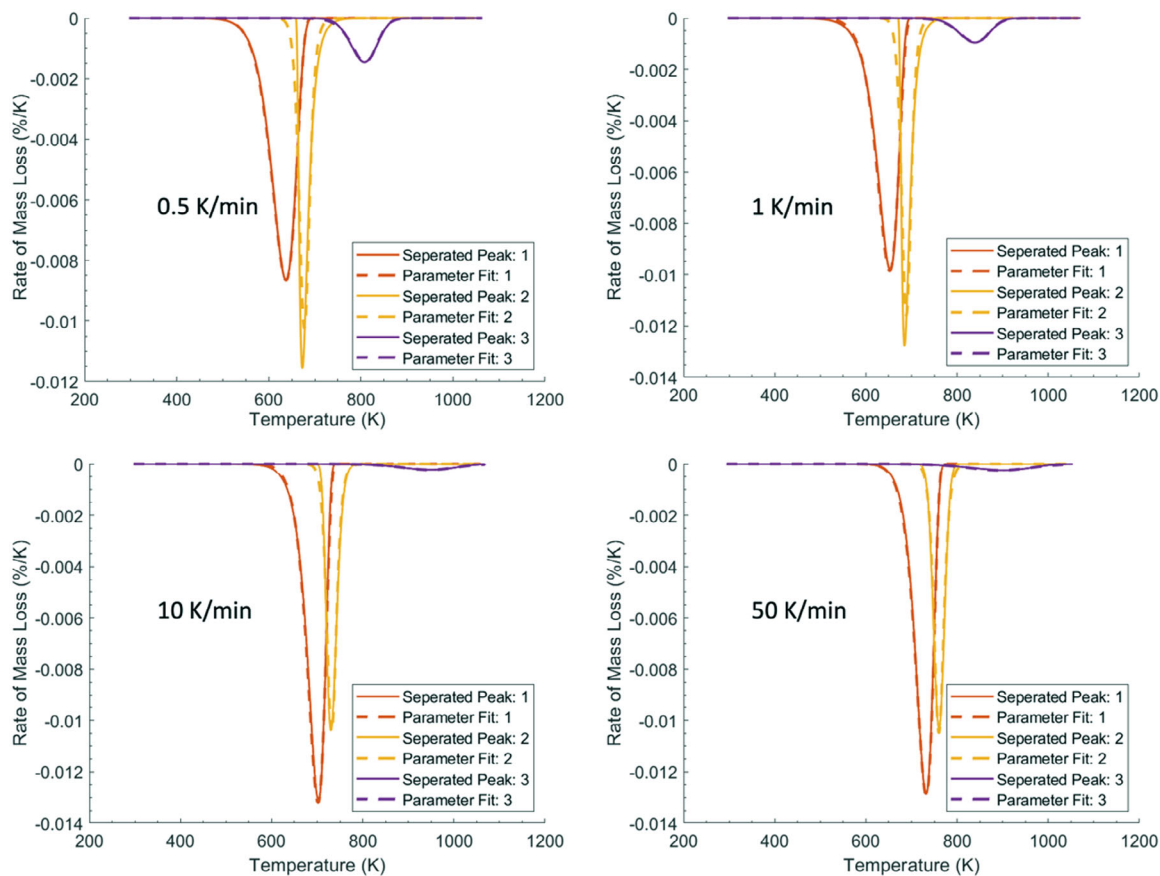
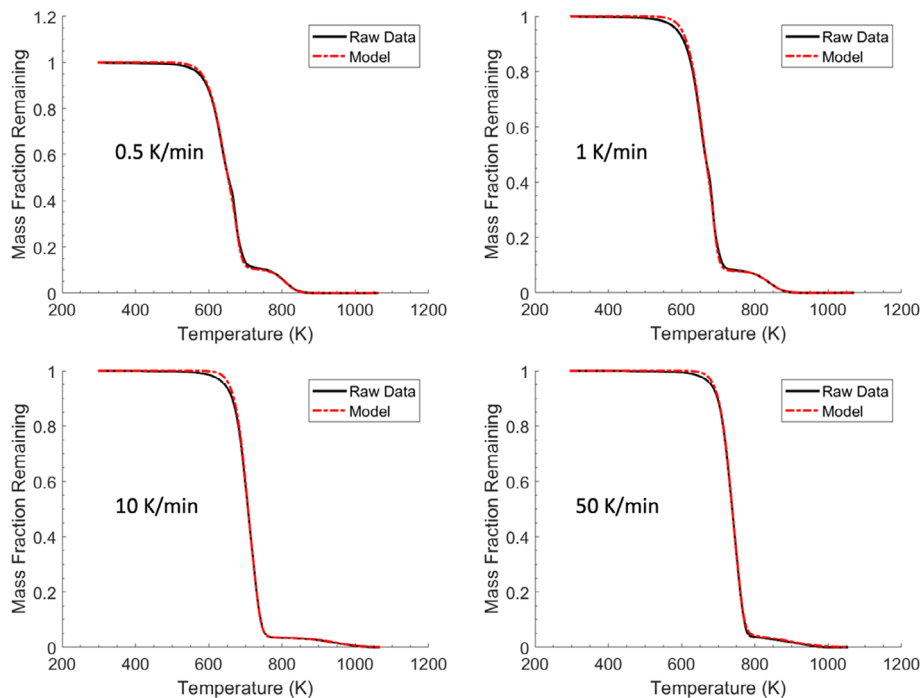
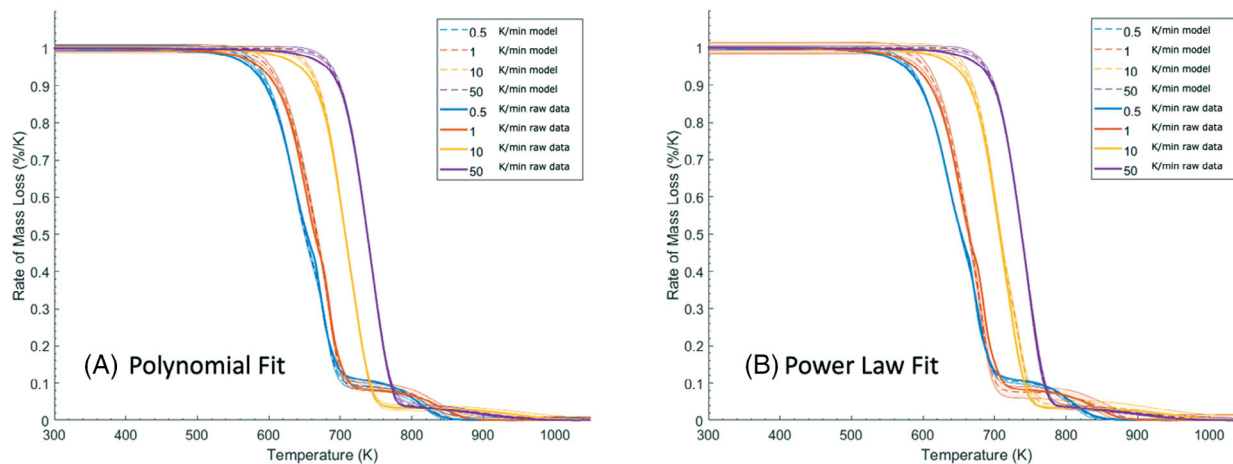


FIGURE 3 Fraser-Suzuki representation (solid lines) and kinetic modeling (dotted lines) of apparent thermal decomposition reactions as a function of heating rate for M100 ceramic vat photopolymerization (CerVPP) 3D printing resin.



**FIGURE 4** Predicted conversion factors as computed using Equation (7) in conjunction with the data in Table 1 and its comparison with the raw thermogravimetric analysis (TGA) data for M100 ceramic vat photopolymerization (CerVPP) resin.



**FIGURE 5** Thermogravimetric analysis (TGA) data with (a) polynomial fit and (b) power law fit M100 ceramic vat photopolymerization (CerVPP) 3D printing resin.

data and depicted in Figure 4. The match between the raw data and the prediction of the model is satisfactory.

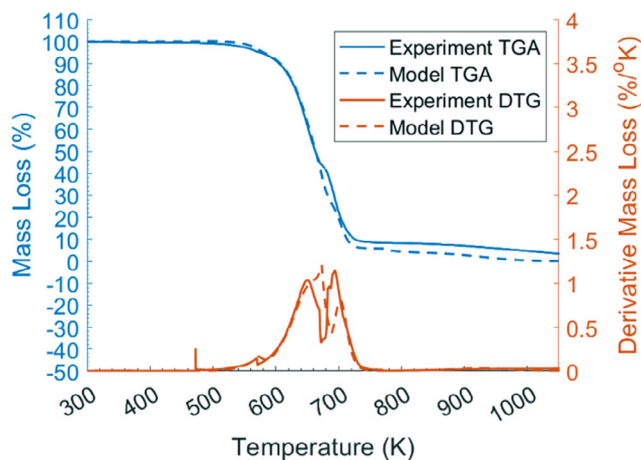
With kinetic parameters established across measured heating rates, there is a need to predict behaviors at intermediate heating rates. Two approaches were explored to describe the kinetic parameters as a function of heating rate: (1) a second order polynomial fit, and (2) a power law fit. These fits were aimed at finding the relative peak weight, pre-exponential factor, and activation energy as a function of heating rate. Comparisons against raw TGA data are displayed in Figure 5a for the poly-

nomial and Figure 5b for the power law fits, respectively. Notably, while the polynomial fit exhibits a smaller root mean square error, it describes the frequency factor and activation energy reaching a maximum before the fastest heating rate, justifying a preference for the power law fit in assessing kinetics across varied heating programs.

The overarching goal of this analysis is the search for a model that captures the behaviors of CerVPP resins under diverse heating rates to optimize debinding behavior. As a first effort, this study seeks to produce TGA data for a dynamic heating program—one that encompasses a wide

**TABLE 2** Thermal treatment cycles used for modeling of thermal decomposition.

Heating step	Heating rate (K/min)	Final temperature (K)
1	5	473
2	0.5	573
3	1	573
4	2	773
5	10	1073

**FIGURE 6** Comparison of the thermal decomposition kinetics model for thermogravimetric analysis (TGA) and differential thermogravimetry (DTG) and the experimental data for M100 ceramic vat photopolymerization (CerVPP) 3D printing resin.

range of heating rates of practical interest. This program, as illustrated in Table 2, was created to mimic a typical debinding protocols, starting with rapid heating that decelerates around the peak degradation rate and then accelerates near the completion of degradation.

A MATLAB program was employed to evaluate the concentration ( $\alpha$ ) as a function of temperature for the designed heating schedule. This program first determines the kinetic parameters at each heating rate step with the power law fit to the kinetic parameters discussed previously. To prevent large discontinuities between heating rate steps, an interpolation procedure was applied at the beginning of each step. This involves linearly interpolating the kinetic parameters and peak weights over the initial 33% of the temperature range of the current ramp, creating a smooth transition between the old and new heating rates and parameters. The program then determines the concentration change at each heating rate step using the finite difference solution.

As illustrated in Figure 6, the model captures the experimental sample's behavior, highlighting two prominent reaction rate peaks. However, there are some notable

discrepancies: an extended elevated rate for the first degradation step. The temperatures at which the peak degradation rates occur do not precisely match, and a zero mass is reached at the final temperature. These discrepancies could be attributed to several factors. First, there might be errors in the individual heating rate models fitted to the experimental data. This could be due to a limitation of the chosen reaction model, the existence more than three main reactions, or reactions that are not independent. Second, the power law description of the dependence of the kinetic parameters might not be adequate. Third, the use of linear interpolation between heating rates could introduce some inaccuracies as it may not capture how the temperature controller transitions between heating rates. Last, there may be residual carbon left in the sample at the conclusion of heating, which the model does not consider. All these factors contribute to the differences observed between the model predictions and the experimental data. Further work is needed to address these potential issues and refine the model. Next steps could involve using hyphenated TGA methods, such as TGA-MS and TGA-FTIR, to identify specific reaction products and their concentrations. This would clarify the constituent reactions contributing to the apparent reaction steps. A better understanding of the degradation mechanisms could improve modeling of the relationship between heating rate and kinetic parameters. Additional heating rate experiments may also highlight the link between apparent reaction steps and underlying reactions. Another enhancement would be relating the predicted generation of gas products to the internal pressure experienced in a ceramic green body. This study does not account for gas transport, which plays a significant role in binder removal. Nevertheless, despite these complexities, the simplified model presented here provides a sufficient fit for practical applications.

## 5 | CONCLUDING REMARKS

This study provided insights into the thermal decomposition kinetics of a simplified CerVPP resin at different heating rates. The decomposition of this resin, as studied by TGA, revealed three main apparent reaction steps, identified using peaks in the rate of mass loss. These apparent reactions were treated as independent from each other. Mass loss peaks were deconvolved using the Fraser–Suzuki function. It was shown that peak deconvolution using this function was effective in modeling DTG peaks, particularly at a 0.5 K/min heating rate. The DTG data were deconvolved into three apparent decomposition steps. Kinetic model fitting using non-linear regression was applied to each deconvolved apparent reaction step. The kinetic model identified a reaction order, activation energy,

and pre-exponential factor for each deconvolved reaction peak. The relationship between the kinetic parameters and heating rate was explored by comparing power law and second-order polynomial relationships. The developed model was shown to be capable of predicting the two main apparent reaction peaks, measured using DTG, of thermal debinding using a multi-segment heating rate program. When used by itself, this model can allow a practitioner to quickly develop a heating rate program that has a wide decomposition range, which allows time for the gas generated during debinding to escape. This model could also be combined with a gas transport model to tie the predicted thermal behavior to pressure gradients in the part that are often the source of cracking and delamination. Future work should include a more thorough understanding of ceramic–resin interactions, specific reaction mechanisms, and the inclusion of isothermal treatments. Ultimately, this study contributes to the ongoing effort to develop more accurate and reliable models for predicting the thermal decomposition of materials, which is essential for improving the binder removal process in CerVPP and optimizing thermal processes in general.

## ACKNOWLEDGMENTS

The authors are thankful for the financial support provided by the National Science Foundation (I/UCRC award 1540027). The views and conclusions contained in this document are those of the authors and should not be interpreted as representing the official policies, either expressed or implied, of the National Science Foundation. The authors would also like to thank Kieran McAleer for his assistance editing and proofreading this manuscript.

## ORCID

Enver Koray Akdoğan  <https://orcid.org/0000-0002-4716-0090>

## REFERENCES

- Lakhdar Y, Tuck C, Binner J, Terry A, Goodridge R. Additive manufacturing of advanced ceramic materials. *Prog Mater Sci.* 2021;116:100736. <https://doi.org/10.1016/j.pmatsci.2020.100736>
- Zhang L, Huang J, Xiao Z, Yu H, Kaige L, Bin H, et al. Effects of debinding condition on microstructure and densification of alumina ceramics shaped with photopolymerization-based additive manufacturing technology. *Ceram Int.* 2022;48(10):14026–38. <https://doi.org/10.1016/j.ceramint.2022.01.288>
- Gu Q, Wang H, Gao W, Yu J, Zhou X. Preparation of large-size alumina ceramic parts by DLP 3D printing using high-solid-loading paste and optimizing the debinding process. *Ceram Int.* 2023;49(17, part B):28801–12. <https://doi.org/10.1016/j.ceramint.2023.06.142>
- Buggakupta W, Wasanapiarnpong T, Chuankrerkkul N. Debinding behaviour and sintering temperature-dependent features of coloured zirconia fabricated by ceramic injection moulding. *J Met Mater Miner.* 2021;31(2):84–88. <https://doi.org/10.55713/jmmm.v31i2.1056>
- Archodoulaki V-M, Koch T, Jones MP. Thermo(oxidative) stability of polymeric materials. *Thermal analysis of polymeric materials.* John Wiley & Sons, Ltd.; 2022. p. 353–79. <https://doi.org/10.1002/9783527828692.ch9>
- Setter R, Schmölzer S, Rudolph N, Moukhina E, Wudy K. Thermal stability and curing behavior of acrylate photopolymers for additive manufacturing. *Polym Eng Sci.* 2023;63(7):2180–92. <https://doi.org/10.1002/pen.26355>
- McAleer EG, Alazzawi MK, Hwang C, LaManna JM, Jacobson DL, Khaykovich B, et al. Binder removal from ceramic stereolithography green bodies: a neutron imaging and thermal analysis study. *J Am Ceram Soc.* 2023;106(7):4399–410. <https://doi.org/10.1111/jace.19095>
- Wang K, Qiu M, Jiao C, Gu J, Xie D, Wang C, et al. Study on defect-free debinding green body of ceramic formed by DLP technology. *Ceram Int.* 2020;46(2):2438–46. <https://doi.org/10.1016/j.ceramint.2019.09.237>
- Zubrzycka P, Radecka M, Graule T, Stuer M. Debinding of additively manufactured parts from spinel powders with particle sizes below 200 nm. *Ceram Int.* 2023;49(7):11355–67. <https://doi.org/10.1016/j.ceramint.2022.11.335>
- Lombardo SJ, Retzlaff DG. Reaction–permeability optimum time heating policy via process control for debinding green ceramic components. *Adv Appl Ceram.* 2020;119(3):150–57. <https://doi.org/10.1080/17436753.2019.1707393>
- Enneti RK, Park SJ, German RM, Atre SV. Review: thermal debinding process in particulate materials processing. *Mater Manuf Processes.* 2012;27(2):103–18. <https://doi.org/10.1080/10426914.2011.560233>
- Li H, Liu Y, Liu Y, Zeng Q, Hu K, Lu Z, et al. Effect of debinding temperature under an argon atmosphere on the microstructure and properties of 3D-printed alumina ceramics. *Mater Character.* 2020;168:110548. <https://doi.org/10.1016/j.matchar.2020.110548>
- Goswami A, Srivastava G, Umarji AM, Madras G. Thermal degradation kinetics of poly(trimethylol propane triacrylate)/poly(hexane diol diacrylate) interpenetrating polymer network. *Thermochim Acta.* 2012;547:53–61. <https://doi.org/10.1016/j.tca.2012.08.006>
- Abdelkader M, Petrik S, Nestler D, Fijalkowski M. Ceramics 3D printing: a comprehensive overview and applications, with brief insights into industry and market. *Ceramics.* 2024;7(1):68–85. <https://doi.org/10.3390/ceramics7010006>
- Vyazovkin S, Burnham AK, Criado JM, Pérez-Maqueda LA, Popescu C, Sbirrazzuoli N. ICTAC Kinetics Committee recommendations for performing kinetic computations on thermal analysis data. *Thermochim Acta.* 2011;520(1):1–19. <https://doi.org/10.1016/j.tca.2011.03.034>
- Coats AW, Redfern JP. Thermogravimetric analysis. A review. *Analyst.* 1963;88(1053):906. <https://doi.org/10.1039/an9638800906>
- Lee T, Beck S. A new integral approximation formula for kinetic analysis of nonisothermal TGA data. *AIChE J.* 1984;30:517–19. <https://doi.org/10.1002/aic.690300332>
- Kissinger HE. Reaction kinetics in differential thermal analysis. *Anal Chem.* 1957;29(11):1702–6. <https://doi.org/10.1021/ac60131a045>

19. Flynn JH, Wall LA. General treatment of the thermogravimetry of polymers. *J Res Natl Bur Stand A Phys Chem.* 1966;70A(6):487–523. <https://doi.org/10.6028/jres.070A.043>
20. Cai J, Yao F, Yi W, He F. New temperature integral approximation for nonisothermal kinetics. *AIChE J.* 2006;52(4):1554–57. <https://doi.org/10.1002/aic.10732>
21. Vyazovkin S, Burnham AK, Favregeon L, Koga N, Moukhina E, Pérez-Maqueda LA, et al. ICTAC Kinetics Committee recommendations for analysis of multi-step kinetics. *Thermochim Acta.* 2020;689:178597. <https://doi.org/10.1016/j.tca.2020.178597>
22. Pijolat M, Soustelle M. Experimental tests to validate the rate-limiting step assumption used in the kinetic analysis of solid-state reactions. *Thermochim Acta.* 2008;478(1):34–40. <https://doi.org/10.1016/j.tca.2008.08.013>
23. Kissinger HE. Differential thermal analysis. *J Res Natl Bur Stand.* 1956;57(4):217.
24. Jaw K-S, Hsu C-K, Lee J-S. The thermal decomposition behaviors of stearic acid, paraffin wax and polyvinyl butyral. *Thermochim Acta.* 2001;367–368:165–68. [https://doi.org/10.1016/S0040-6031\(00\)00680-8](https://doi.org/10.1016/S0040-6031(00)00680-8)
25. Yao F, Wu Q, Lei Y, Guo W, Xu Y. Thermal decomposition kinetics of natural fibers: activation energy with dynamic thermogravimetric analysis. *Polym Degrad Stab.* 2008;93(1):90–98. <https://doi.org/10.1016/j.polymdegradstab.2007.10.012>
26. García-Garrido C, Pérez-Maqueda LA, Criado JM, Sánchez-Jiménez PE. Combined kinetic analysis of multistep processes of thermal decomposition of polydimethylsiloxane silicone. *Polymer.* 2018;153:558–64. <https://doi.org/10.1016/j.polymer.2018.08.045>
27. Budrugaec P. A simple and precise differential incremental isoconversional method to kinetic analysis of heterogeneous processes under arbitrary temperature programs. *Thermochim Acta.* 2018;661:116–23. <https://doi.org/10.1016/j.tca.2018.01.025>
28. Friedman HL. Kinetics of thermal degradation of char-forming plastics from thermogravimetry. Application to a phenolic plastic. *J Polym Sci C Polym Symp.* 1964;6(1):183–95. <https://doi.org/10.1002/polc.5070060121>
29. Ozawa T. A new method of analyzing thermogravimetric data. *Bull Chem Soc Jpn.* 1965;38(11):1881–86. <https://doi.org/10.1246/bcsj.38.1881>
30. Wang F-Y, Ma C-CM, Wu W-J. Kinetic parameters of thermal degradation of polyethylene glycol-toughened novolac-type phenolic resin. *J Appl Polym Sci.* 2001;80(2):188–96. [https://doi.org/10.1002/1097-4628\(20010411\)80:2<188::AID-APP1086>3.0.CO;2-B](https://doi.org/10.1002/1097-4628(20010411)80:2<188::AID-APP1086>3.0.CO;2-B)
31. Vyazovkin S. Evaluation of activation energy of thermally stimulated solid-state reactions under arbitrary variation of temperature. *J Comput Chem.* 1997;18(3):393–402. [https://doi.org/10.1002/\(SICI\)1096-987X\(199702\)18:3<393::AID-JCC9>3.0.CO;2-P](https://doi.org/10.1002/(SICI)1096-987X(199702)18:3<393::AID-JCC9>3.0.CO;2-P)
32. Vyazovkin S. Modification of the integral isoconversional method to account for variation in the activation energy. *J Comput Chem.* 2001;22(2):178–83. [https://doi.org/10.1002/1096-987X\(20010130\)22:2%3C178::AID-JCC5%3E3.0.CO;2-%23](https://doi.org/10.1002/1096-987X(20010130)22:2%3C178::AID-JCC5%3E3.0.CO;2-%23)
33. Vyazovkin S, Sbirrazzuoli N. Isoconversional kinetic analysis of thermally stimulated processes in polymers. *Macromol Rapid Commun.* 2006;27(18):1515–32. <https://doi.org/10.1002/marc.200600404>
34. Saha B, Ghoshal AK. Thermal degradation kinetics of poly(ethylene terephthalate) from waste soft drinks bottles. *Chem Eng J.* 2005;111(1):39–43. <https://doi.org/10.1016/j.cej.2005.04.018>
35. Prati JL. Modeling polymeric binder degradation for transport through porous green bodies. Rutgers University; 2017. <https://doi.org/10.7282/T3CJ8HNS>
36. Gavin HP. The Levenberg–Marquardt algorithm for nonlinear least squares curve-fitting problems. Department of Civil and Environmental Engineering, Duke University; 2019. p. 19.
37. Conn AR, Gould NIM, Toint PL. Trust region methods. Society for Industrial and Applied Mathematics; 2000.
38. Laidler KJ. Chemical kinetics. Harper & Row; 1987.
39. Cheng Z, Wu W, Ji P, Zhou X, Liu R, Cai J. Applicability of Fraser–Suzuki function in kinetic analysis of DAEM processes and lignocellulosic biomass pyrolysis processes. *J Therm Anal Calorim.* 2015;119(2):1429–38. <https://doi.org/10.1007/s10973-014-4215-3>
40. Hu M, Chen Z, Wang S, Guo D, Ma C, Zhou Y, et al. Thermogravimetric kinetics of lignocellulosic biomass slow pyrolysis using distributed activation energy model, Fraser–Suzuki deconvolution, and iso-conversional method. *Energy Convers Manag.* 2016;118:1–11. <https://doi.org/10.1016/j.enconman.2016.03.058>
41. Svoboda R, Málek J. Applicability of Fraser–Suzuki function in kinetic analysis of complex crystallization processes. *J Therm Anal Calorim.* 2013;111(2):1045–56. <https://doi.org/10.1007/s10973-012-2445-9>
42. Fraser RDB, Suzuki E. Resolution of overlapping bands. Functions for simulating band shapes. *Anal Chem.* 1969;41(1):37–39. <https://doi.org/10.1021/ac60270a007>
43. Fraser RD, Suzuki E. Resolution of overlapping absorption bands by least squares procedures. *Anal Chem.* 1966;38(12):1770–73.
44. O’Haver T. A pragmatic introduction to signal processing with applications in scientific measurement. University of Maryland at College Park; 2015. p. 74.
45. Lagarias JC, Reeds JA, Wright MH, Wright PE. Convergence properties of the Nelder–Mead simplex method in low dimensions. *SIAM J Optim.* 1998;9(1):112–47. <https://doi.org/10.1137/S1052623496303470>
46. Vyazovkin S, Chrissafis K, Di Lorenzo ML, N Koga, M Pijolat, B Roduit, et al. ICTAC Kinetics Committee recommendations for collecting experimental thermal analysis data for kinetic computations. *Thermochim Acta.* 2014;590:1–23. <https://doi.org/10.1016/j.tca.2014.05.036>

**How to cite this article:** McAleer EG, Prati J, Matthewson JM, Haber RA, Akdoğan EK. Predicting photopolymer resin pyrolysis kinetics in ceramic vat photopolymerization additive manufacturing. *J Am Ceram Soc.* 2025;e20470. <https://doi.org/10.1111/jace.20470>